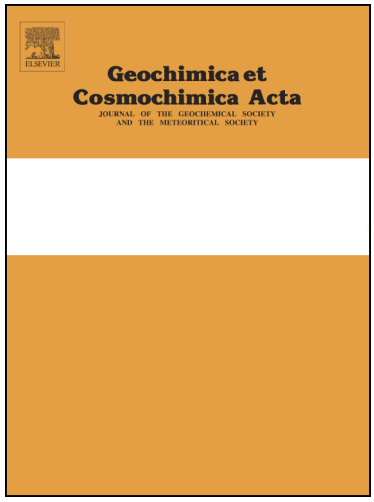

Effects of soluble flavin on heterogeneous electron transfer between surface-exposed bacterial cytochromes and iron oxides

Zheming Wang, Zhi Shi, Liang Shi, Gaye F. White, David J. Richardson, Thomas A. Clarke, Jim K. Fredrickson, John M. Zachara

PII: S0016-7037(15)00191-X
DOI: http://dx.doi.org/10.1016/j.gca.2015.03.039
Reference: GCA 9204

To appear in: *Geochimica et Cosmochimica Acta*

Received Date: 27 October 2014
Accepted Date: 28 March 2015

Please cite this article as: Wang, Z., Shi, Z., Shi, L., White, G.F., Richardson, D.J., Clarke, T.A., Fredrickson, J.K., Zachara, J.M., Effects of soluble flavin on heterogeneous electron transfer between surface-exposed bacterial cytochromes and iron oxides, *Geochimica et Cosmochimica Acta* (2015), doi: http://dx.doi.org/10.1016/j.gca.2015.03.039

Effects of soluble flavin on heterogeneous electron transfer between surface-exposed bacterial cytochromes and iron oxides

Zheming Wang,[†*] *Zhi Shi*,[†] *Liang Shi*,[†] *Gaye F. White*,[‡] *David J. Richardson*,[‡] *Thomas A. Clarke*,[‡] *Jim K. Fredrickson*,[†] *John M. Zachara*[†*]

[†]Pacific Northwest National Laboratory, PO Box 999, MS K8-96, Richland, WA 99352

[‡]Centre for Molecular and Structural Biochemistry, School of Biological Sciences and School of Chemistry, University of East Anglia, Norwich NR4 7TJ, United Kingdom

[*] Corresponding authors: Zheming Wang, Pacific Northwest National Laboratory, MS K8-96, Richland, WA 99354; Phone: (509) 371-6349; Fax: (509) 371-6354; E-mail: zheming.wang@pnnl.gov; John M. Zachara, phone: 1-509-371-6355, fax: 1-509-371-6354; Email: john.zachara@pnnl.gov.

Geochimica et Cosmochimica Acta

ABSTRACT

Dissimilatory iron-reducing bacteria can utilize insoluble Fe(Mn)-oxides as a terminal electron acceptor under anaerobic conditions. For *Shewanella* species specifically, multiple evidences suggest that iron reduction is associated with the secretion of flavin mononucleotide (FMN) and riboflavin. However, the exact mechanism of flavin involvement is unclear; while some indicate that flavins mediate electron transfer (Marsili et al., 2008), others point to flavin serving as co-factors to outer membrane proteins (Okamoto et al., 2013). In this work, we used methyl viologen ($MV^{\bullet+}$)-encapsulated, porin-cytochrome complex (MtrCAB) embedded liposomes (MELs) as a synthetic model of the *Shewanella* outer membrane to investigate the proposed mediating behavior of microbially produced flavins. The reduction kinetics of goethite, hematite and lepidocrocite (200 μM) by MELs ($[MV^{\bullet+}] \sim 42$ μM and MtrABC ≤ 1 nM) were determined in the presence FMN at pH 7.0 in N_2 atmosphere by monitoring the concentrations of $MV^{\bullet+}$ and FMN through their characteristic UV-visible absorption spectra. Experiments were performed where i) FMN and Fe(III)-oxide were mixed and then reacted with the reduced MELs and ii) FMN was reacted with the reduced MELs followed by addition of Fe(III)-oxide. The redox reactions proceeded in two steps: a fast step that was completed in a few seconds, and a slower one lasting over 400 seconds. For all three Fe(III)-oxides, the initial reaction rate in the presence of a low concentration of FMN (≤ 1 μM) was at least a factor of five faster than those with MELs alone, and orders of magnitude faster than those by $FMNH_2$, suggesting that FMN may serve as a co-factor that enhances electron transfer from outer-membrane *c*-cytochromes to Fe(III)-oxides. The rate and extent of the initial reaction followed the order of lepidocrocite > hematite > goethite, the same as their reduction potentials, implying thermodynamic control on reaction rate. For LEP, with the highest reduction potential among the three Fe(III)-oxides, its reduction by $FMNH_2$ completed in less than 10 minutes, suggesting that FMN is capable of

mediating electron transfer to LEP. At higher FMN concentrations (> 1 μM), the reaction rates for both steps decreased and varied inversely with FMN concentration, indicating that FMN inhibited the MEL to Fe(III)-oxide electron transfer reaction under these conditions. The implications of the observed kinetic behaviors to flavin-mediated Fe(III) oxide reduction in natural environments are discussed.

1. INTRODUCTION

Dissimilatory iron reduction (DIR) by bacteria, which is linked to the reductive dissolution of Fe(III) oxides is a key component of the iron biogeochemical cycle ((Lovley et al., 1987; Roden and Zachara, 1996; Zachara et al., 2001)). At the heart of this process is extracellular and interfacial electron transfer between dissimilatory iron reducing bacteria (DIRB) and Fe(III) containing mineral phases that determines iron valence and solubility. A detailed understanding of the mechanisms of dissimilatory iron reduction has arisen primarily from the study of two model organism species: *Shewanella and Geobacter* (Lovley, 1991; Myers and Nealson, 1988; Myers and Nealson, 1990). These organisms differ in the geochemical environments that they populate, electron donors utilized, molecular machinery for DIR, and other ecologic aspects.

MR-1 and related strains of metal-reducing *Shewanella* have evolved the Mtr pathway for extracellular electron transfer (Clarke et al., 2011; Lies et al., 2005; Ross et al., 2009; Ross et al., 2007). Details of the Mtr pathway of MR-1 have been recently revealed (Clarke et al., 2011; Hartshorne et al., 2009; Shi et al., 2007). Homologues of the Mtr pathway are present in *Geobacter* (Liu et al., 2014) and Fe(II)-oxidizing bacteria (Shi et al., 2012b; Shi et al., 2012c), attesting to the generality of its mechanism and function. The protein components of the Mtr pathway of *S. oneidensis* MR-1 include multi-heme, *c*-type cytochromes (*c*-Cyts), CymA, MtrA(D), MtrC(F) and OmcA; and a trans-membrane, porin-like protein MtrB(E)[Note MR-1

has redundant gene clusters for the Mtr pathway giving rise to two distinct but closely similar protein series: MtrCAB and MtrFDE (Clarke et al., 2011) that form functional ternary molecular complexes (Richardson et al., 2012)]. CymA is a dehydrogenase that oxidizes quinol in the inner-membrane and transfers electrons to MtrA(D) either directly or indirectly via other periplasmic proteins. MtrA(D) inserts into porin protein MtrB(E) that spans the outer membrane. Outer membrane-bound MtrC(F) interact with MtrA(D) to form a ternary complex that functions as a terminal reductase for electron transfer to Fe(III) solids (for recent reviews, see (Richardson et al., 2012; Shi et al., 2012a)).

Recent studies suggest that microbially produced soluble flavins can mediate electron transfer between the Mtr-pathway and Fe(III)-containing mineral phases. An electron shuttle mechanism is proposed (Brutinel and Gralnick, 2012). Within context of this study, an electron shuttle is defined as a relatively low molecular weight redox active molecule. Shuttles have favorable reaction properties for Fe(III) oxides and may diffuse into intra-aggregate or intra-grain space not accessible to whole cells and have reaction kinetics that are not strongly constrained by the approach distance and orientation relative to outer membrane *c*-type cytochromes (Breuer et al., 2014; Brutinel and Gralnick, 2012). The shuttle hypothesis is based on circumstantial observations that (i) crystallized MtrF display a putative flavin-binding motif in their structure (Clarke et al., 2011), ii.) the Mtr pathway is required for extracellular reduction of flavins (Coursolle et al., 2010a; Coursolle et al., 2010b), (iii) purified MtrC and OmcA reduce flavins with subsequent electron transfer to Fe(III)(Ross et al., 2009; Shi et al., 2012c), (iv) higher flavin concentrations are associated with cell growth under anaerobic conditions where DIR occurs, and (v) addition of flavins to growth media enhance the reduction of poorly crystalline Fe(III) oxides (von Canstein et al., 2008; Wu et al., 2013). However, there has been

no conclusive evidence to verify the mechanism by which flavin enhances Fe(III) oxide reductive dissolution as its apparent effect could be associated with other undetermined factors within the growth media. It is additionally unclear whether the mediating effect of flavin applies to all Fe(III)-oxides which vary in reduction potentials (Table 1) at more oxidizing values than those of flavins. The reduction rates of goethite by reduced flavin mononucleotide ($FMNH_2$; E' = -.216 V; 0.001 µmol m^{-2} s^{-1}), for example, were three orders of magnitude slower than lepidocrocite (1.1 µmol m^{-2} s^{-1})(Shi et al., 2012c; Shi et al., 2013). Thus, mediation efficiency may be dependent on the nature of Fe(III) oxides present in the geochemical system of interest.

We recently demonstrated a MtrCAB proteoliposome system for investigating interfacial electron transfer reactions between outer membrane cytochromes and mineral phases (White et al., 2012; White et al., 2013). The MtrCAB complex is embedded within the lipid bilayer with MtrC exposed on the outer surface of the liposome and MtrA on the inside, mimicking the *in vivo* organization of the MtrCAB electron transfer conduit between the periplasm and the outer membrane (Clarke et al., 2011; Ross et al., 2007; White et al., 2013). The methyl viologen cation (MV^{2+}), a redox-sensitive dye and strong reductant (E^0 = -0.450 V), is encapsulated within the liposome to drive and monitor transmembrane electron transfer (Hartshorne et al., 2009; White et al., 2012). Encapsulated MV^{2+} is readily reduced to $MV^{\bullet+}$ through the molecular conduit by stoichiometric addition of sodium dithionite outside of the proteoliposomes. The resulting $MV^{\bullet+}$-containing proteoliposomes reduce both aqueous ferric complexes and suspended iron (III) oxides. The reduction rates of Fe(III) oxides by the $\underline{M}V^{\bullet+}$-encapsulated, porin cytochrome complex $\underline{M}$trCAB-$\underline{e}$mbedded $\underline{l}$iposomes (White et al., 2013) (termed MELs) were 2 to 3 orders of magnitude faster than that by MtrC alone (Ross et al., 2009), albeit under different experimental conditions.

In typical *in vitro* studies of Fe(III)-oxide reductive dissolution by isolated outer-membrane proteins or flavins, the reductant molecules are rapidly oxidized upon addition of oxidant and the effective redox potential continuously increases as the reductant is oxidized (Ross et al., 2009; Shi et al., 2012c; Shi et al., 2013; Wang et al., 2008). The MEL system with encapsulated $MV^{\bullet+}$, in contrast, provides a reservoir of reductant with relatively constant reduction potential that is regulated by the redox properties of the outer-membrane proteins (redox window of -0.400 - 0.000 V (Hartshorne et al., 2009)) that span the lipid bilayer. The outer membrane proteins, owing to their low concentration in the MEL suspension (e.g. ~ 1 nM) relative to $MV^{\bullet+}$ (~42 μM), experience a high redox turnover rate that simulates the *in vivo* bacterial system that is driven by metabolism. Consequently, the MEL system represents an experimental platform to evaluate select reaction mechanisms and kinetics of electron transfer enhancement that is free from the complicating effects of alternative electron transfer pathways, diffusive limitations to electron acceptor availability, other secreted organic molecules, growth, and lysis that complicate whole cell studies.

Here we report on the reduction kinetics of goethite (GT), hematite (HT) and lepidocrocite (LEP) by MELs in the presence of FMN under chemically constrained conditions to evaluate the potential accelerating role of FMN in the extracellular reduction of Fe(III) oxides. We examined the effects of FMN concentration and iron oxide phase identity, free energy (half-cell potential), and concentration on the reductive dissolution rate. Evidence was explicitly sought for reductive dissolution rate enhancement by FMN and the conditions under which this occurred. The resulting experimental observations allowed us to refine a mechanistic understanding of the impacts of microbially produced flavins on bacterial iron oxide reduction in a complex model system.

2. EXPERIMENTAL

2.1 Materials and Methods

Phosphatidylcholine, valinomycin, flavin mononucleotide (FMN), sodium dithionite (sodium hydrosulfite, technical grade, 85%), methyl viologen dichloride, ferrozine reagent (3-(2-Pyridyl)-5,6-diphenyl-1,2,4-triazine-4',4''-disulfonic acid sodium salt), and HEPES, were obtained from Sigma-Aldrich. Distilled, deionized water (DDW) with a resistivity of 18 MΩ-cm (Barnstead Nanopure) was used for all experiments. Bottles and glassware were soaked in 2 M hydrochloric acid (Sigma-Aldrich), rinsed with distilled water, soaked in 5 M nitric acid (Fisher Scientific), rinsed with distilled water, and then rinsed with DDW and air dried.

2.2 Syntheses and characterization of Fe(III) oxides

GT, HT, and LEP were synthesized according to the methods of Schwertmann and Cornell (Schwertmann and Cornell, 2000). Details of the syntheses, washing, and the resulting material properties have been provided elsewhere (c; Shi et al., 2013). Reduction potential, surface area, and pH_{pzc} values of the Fe(III)-oxides are listed in Table 1.

2.3 Preparation of MELs

MELs with concentrations of MV^{2+} ~42 μM and MtrCAB (≤ 1 nM) were prepared according to the method of White et al. (White et al., 2012; White et al., 2013). Fresh MELs were stored at 4 ℃ and used within two weeks after preparation.

2.4 Experimental design and data analysis

Batch experiments were conducted under conditions that were similar to those described in White et al (White et al., 2012). In brief, all experiments were conducted in a glovebox (100% N_2 atmosphere, Innovative Technology, Inc., Amesbury, MA) with strict anaerobic conditions

(oxygen concentration below the detection limit of 0.1 ppm) at 21.0 ± 0.5 C. Deoxygenated, distilled, deionized water (DDDW) was prepared by boiling DDW in a 2 L bottle under vacuum (~ 450 mm Hg vacuum) for 2 hour, and then sparging with high purity nitrogen gas overnight inside the glovebox. The dissolved oxygen concentration in the DDDW was determined with a colorimetric self-filling ampoule (CHEMetrics, Inc.), and the resulting analytical concentration was always below the detection limit (5 ppb) of the colorimetric method. All samples were prepared in 50 mM HEPES buffer (pH 7.0) containing 2 mM $CaCl_2$ and 10 mM KCl. UV-visible spectroscopy measurements were performed in 2.0 mL quartz cuvettes with continuous stirring, and monitored by a Hewlett-Packard model 8543 diode array spectrometer.

The encapsulated methyl viologen radical cation ($MV^{\bullet+}$) functioned as the primary reductant with electron transfer occurring through the MtrABC protein complex. Decrease of the reduced methyl viologen cation ($MV^{\bullet+}$) concentration by oxidation to MV^{2+} was monitored at 606 nm.

MV^{2+} $MV^{+\cdot}$ $E^0 = -0.450$ V (1)

FMN was used as a secondary oxidant for $MV^{\bullet+}$ (in addition to Fe(III) oxide), while its reduced form, $FMNH_2$, served as a secondary or parallel reductant for the Fe(III)-oxides. The $FMN/FMNH_2$ redox pair has a similar but somewhat lower mid-point redox potential than the Fe(III) oxides (Table 1).

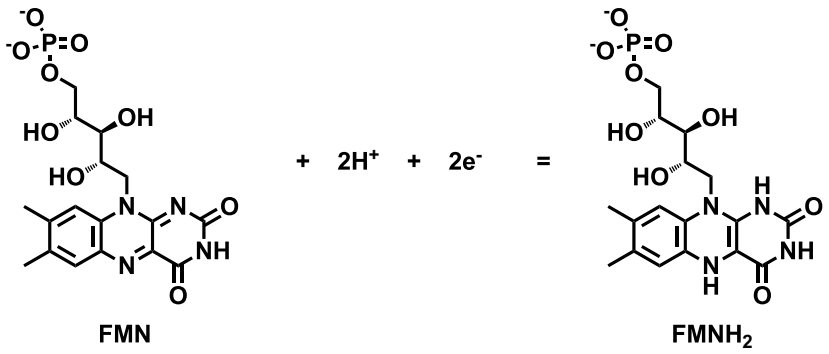

$E^0 = -0.216$ V (2)

The change of FMN concentration was monitored at its characteristic absorption band at 450 nm. Absorbance data were converted to concentrations based on the extinction coefficients of $MV^{\bullet+}$, FMN, $FMNH_2$, and proteoliposomes at the corresponding wavelengths.

The initial concentration of $MV^{\bullet+}$ in the MELs was determined by redox titration with sodium dithionite of known concentration. Preliminary tests indicated that dithionite reduction of MV^{2+} to $MV^{\bullet+}$ in the MELs reached completion within 20 min or less (White et al., 2012). This reaction time was used for MV^{2+} reduction by sodium dithionite in all of the MEL experiments, and the resulting reduced MEL suspensions were used for all the kinetic experiments with FMN and/or Fe(III) oxides. Dithionite additions were carefully performed to minimize post reaction residual concentrations, that could, in turn, have been reactive with the Fe(III) oxides and FMN. Consequently, the concentration of encapsulated $MV^{\bullet+}$ in the working solution was typically slightly less than the total MV concentration ($[MV^{\bullet+}] + [MV^{2+}]$) as measured after decomposition of the MELs (42 μM) with Triton X-100 after completion of the kinetic runs (White et al., 2013).

Two types of kinetic experiments were conducted (Figure S1). FMN and Fe(III) oxide were pre-mixed and quickly added to the MEL system to initiate reaction in the Type I experiment, and the absorbances at 606 nm and 450 nm were monitored for 440 seconds. In the

Type II experiment, FMN alone was added to the MEL suspension, and the reduction of FMN was monitored for 220 seconds. Fe(III) oxide was then added to the suspension, and the reaction was monitored for an additional 440 seconds. Variable concentrations of FMN were used for both the Type I ([FMN] = 0, 1.0, 10.0 and 20 μM) and Type II ([FMN] = 0.001, 0.01, 1.0, 10.0 and 20 μM) experiments with GT. For HT and LEP, Type I and Type II experiments were conducted at [FMN] = 10 μM to allow comparison among the Fe-oxide phases. The resulting Fe(II) concentration was determined by the ferrozine spectrophotometric method (Stookey, 1970). To minimize Fe(II) adsorption on the Fe(III)-oxide-MEL mixtures, ferrozine solution was added to the reaction mixture prior to filtration and spectroscopy analysis.

The initial reaction rate, determined from the slope of the disappearance of the first 10% of the encapsulated $MV^{\bullet+}$ (Shi et al., 2013; Stumm et al., 1985; Torrent et al., 1987; Wang and Newman, 2008), and a second stage reaction rate, defined as the average rate from the inflection point of the initial fast reaction and the slower reaction through 100 seconds, were calculated for comparisons between the three Fe-oxides under different conditions. The 100 second data window was selected to avoid potential measurement errors on the later reaction period for some of the kinetic runs where $MV^{\bullet+}$ concentration within the MELs approached zero and the reaction became extremely slow. The later period accounts for a small fraction of the overall reaction extent. The kinetic data for the Type II experiments were also fitted to a second order reaction model according to Wang et al. (Wang et al., 2008). The second order model was better suited for kinetic analysis of the slower reaction stage. Details of the kinetic analysis approach have been provided elsewhere (Wang et al., 2008).

3. RESULTS

3.1 Type I experiments with goethite

The simultaneous addition of FMN (1, 10 or 20 μM) and GT (200 μM) to the MEL suspension led to the oxidation of the encapsulated $MV^{\bullet+}$ to MV^{2+} within 420 seconds. The electron transfer reactions proceeded in two stages at all three FMN concentration levels: a fast initial stage that was completed within a few seconds and a slower one that took longer than 300 seconds. Separate measurements of the reduction of FMN in the absence of Fe(III) oxide (Figures S2 and S3), or GT in the absence of FMN (Figure 1A) suggested that the fast reaction involved the reduction of both FMN and GT while the slower reaction involved primarily GT. Thus, soluble FMN (E^0 = -0.216 V) reacted faster than nano-particulate GT (E' = -0.158 V) even though the latter was thermodynamically more favorable (Table 1). Monitoring FMN absorbance at 450 nm confirmed its rapid conversion to $FMNH_2$ in the initial reaction stage in both the presence and absence of GT. Thereafter, $FMNH_2$ remained as the dominant flavin species during the entire observation period (Figure 1B). $FMNH_2$ did not appear to react with GT within the experiment time frame, consistent with the slow rate of GT reduction by $FMNH_2$ observed under similar conditions in the absence of MELs (0.001 μM m^{-2} s^{-1}) (Shi et al., 2013). The production of Fe(II) decreased as FMN concentration increased (Figure 1C), indicating preferential electron transfer to FMN rather than GT.

Inspection of the kinetic profiles (Figure 1A) and calculations of reactant/product stoichiometries revealed that FMN affected the reduction of GT differently during the two reaction stages. In the initial stage, where the disappearance rate of $MV^{\bullet+}$ was similar to the reduction rate of FMN alone (Table 2), the drop in $MV^{\bullet+}$ concentration was approximately 10 μM more than the stoichiometric demand from the production of $FMNH_2$ when 1μM and 10 μM FMN were present in the suspension (Figure 1A). The additional oxidation of $MV^{\bullet+}$ could only be attributed to the reduction of GT at greatly enhanced rate. This observation was consistent

with the hypothesis that FMN serves as a co-factor for the reduction of Fe(III)-oxides by *Shewanella* outer-membrane *c*-Cyts (Okamoto et al., 2013) (No molecular mechanism implied). However, in the second stage, the presence of $FMNH_2$ inhibited the reduction of GT. The second stage GT reduction rates decreased from 0.33 μM s^{-1} in the absence of $FMNH_2$ to 0.16 μM s^{-1} and 0.01 μM s^{-1} in the presence 1 μM and 10 μM $FMNH_2$, respectively (Table S1). As a significant portion of GT reduction occurred during the second stage, the overall effect of FMN was to inhibit GT reduction (Figure 1C).

3.2 Type II experiments with goethite

FMN solutions of varying concentration (0, 2 nM, 10 nM, 1 μM, 10 μM and 20 μM) were first reacted with the MELs to completion (e.g., $FMNH_2$) in the Type II experiment. GT was then added to the suspension and its reduction kinetics determined by UV-vis monitoring. Thus, the measured kinetic profiles only involved GT reduction, allowing determination of GT reduction rate without the complication of the concurring fast reduction of FMN. In all cases, the reduction of FMN by the MELs prior to Fe(III) oxide addition was almost instantaneous except with 20 μM FMN, for which a slower stage, similar to that observed in Type I experiment at the same FMN concentration (Figure 1A), was observed (Figures S2 and S3). The addition of 2 nM or 10 nM FMN resulted in initial GT reduction rates (3.29 μM s^{-1} and 3.39 μM s^{-1}, respectively) that were over five times greater than those without FMN (0.59 μM s^{-1}). However, the overall effect of these low FMN concentrations on the kinetic profiles of $MV^{\bullet+}$ oxidation (as compared to [FMN] = 0) was limited (Figure 2A and Table 2).

An increase of FMN to 1 μM led to further enhancement of the initial rate to 8.74 μM s^{-1} (Table 2), while decreasing the second stage reaction rate from ~ 0.33 μM s^{-1} (without FMN) to 0.17 μM s^{-1} (Table S1). An additional increase in FMN to 10 μM led to a further decrease in the

second stage rate (to 0.04 μM s^{-1}, Table S1), and lowering of the initial reaction rate to 3.20 μM s^{-1} (Table 2). At all four FMN concentrations, the measured initial rates were at least five times greater than that in the absence of FMN (Table 2). Because FMN was in the reduced form ($FMNH_2$) prior to GT introduction, the oxidation of $MV^{\bullet+}$ in Figures 2A and 2B only involved electron transfer to GT. The rapid $MV^{\bullet+}$ oxidation during the initial reaction with 2 nM to 10 μM $FMNH_2$ (most evident for 1 and 10 μM Figure 2B) provided unequivocal evidence that $FMNH_2$ interacted with the MtrCAB complex to allow more efficient electron transfer to GT. The reduction of 20 μM FMN prior to goethite addition consumed all the $MV^{\bullet+}$, and thus no further $MV^{\bullet+}$ reaction with GT was observed at this high $FMNH_2$ concentration (Figure 2B). The small amount of $Fe^{2+}_{(aq)}$ observed in the 20 μM $FMNH_2$ experiment (~ 3 μM, Figure 2C) was believed to result from residual dithionite. At all FMN concentration levels, the measured concentration of FMN during the reaction with GT remained at zero (data not shown), indicating little reaction of GT with $FMNH_2$.

A consecutive second-order bimolecular model was applied to simulate the kinetic data given the negligible reaction between $FMNH_2$ and GT (typical data fits are shown in Figure S4). The results revealed that the reduction of GT displayed a single stage bimolecular kinetic reaction with a rate constant of ~ 89 $\mu M^{-1} \cdot s^{-1}$ in the absence of $FMNH_2$. In the presence of reduced $FMNH_2$, all experiments could be modeled by a two-stage bimolecular process with rate constants dependent on the concentration of $FMNH_2$ (Table S2). The rate constants of the initial stage were all over three times higher than those in the absence of $FMNH_2$; they increased with FMN concentration to [$FMNH_2$] = 1 μM, and then decreased at higher $FMNH_2$ concentration. The slower reaction peaked at 10 nM $FMNH_2$ and decreased monotonically as $FMNH_2$ concentration increased. These data trends were consistent with those determined by the initial

(Table 2) and second stage reaction rate analysis (Table S1), supporting the conclusions that $FMNH_2$ i) enhanced the initial reaction rate at low concentrations ($[FMNH_2] \leq 1$ μM), and ii) impeded the second stage reaction at $[FMNH_2] \geq 1$μM.

A comparison of the kinetic data obtained in the Type I and II experiments indicated that the sequence of reactant addition affected the kinetic behavior of the reactions with GT. The initial $MV^{\bullet+}$ oxidation rates were much higher in Type I experiment than those in Type II experiment at the same FMN concentration (10 μM) because of rapid, FMN reduction. On the other hand, the reaction rates in the Type II experiment were descriptive of the fundamental kinetic interaction between the $FMNH_2$-modified MEL reductants and GT.

3.3 Reductive dissolution of hematite and lepidocrocite in MELs suspensions

Type I and Type II experiments were performed using HT and LEP under the same conditions used for GT with FMN at 10 μM. Control experiments in the absence of FMN demonstrated that the reduction rates by MELs followed the order of GT < HT < LEP (Figures 2A, 3A and 4A; Table 2) as reported previously (White et al., 2013).

3.3.1 Type I Experiments The reaction of HT and LEP displayed similar patterns to that of GT, with an initial rapid drop of $MV^{+\bullet}$ concentration from ~ 40 μM to ~ 11 μM, followed by a reaction stage that was slower than that in the absence of FMN (Figures 3A and 4A). For GT, there was a lag period between the initial and slower stages of reactions (Figure 1A). The lag period was much shorter for HT and non-existent for LEP, likely caused by the greater thermodynamic driving force for the latter reaction pairs. The initial rates were all fast due to the dominance of fast FMN reduction by MELs during this period (Table 2) while the second stage reaction rates were smaller than those in the absence of FMN (Table S1). Among the three

Fe(III)-oxides, the second stage rates increased from GT (0.01 μM s^{-1}) to HT (0.05 μM s^{-1}) to LEP (0.12 μM s^{-1}).

Pronounced differences were observed in the FMN concentration profiles over the course of the reaction for HT and LEP as compared to GT (Figs. 1B, 3B and 4B). While FMN was quickly reduced and remained as $FMNH_2$ during reaction with GT, [FMN] dropped to ~ 3 μM during the initial reaction in the mixture with HT with the remaining FMN reduced slowly (Figure 3B). In the reaction with LEP, the concentration of FMN displayed a momentary concentration dip to ~ 4.2 μM at the beginning of the reaction, followed by an immediate rebound to nearly the starting FMN concentration; only a marginal additional decrease was observed during the remainder of the reaction period (Figure 4B). The concentration rebound of FMN suggested $FMNH_2$ oxidation by reaction with LEP. This result was consistent with rapid measured rates of $FMNH_2$ reaction with LEP in the absence of MELs ($r_{initial}$ = 1.3 μM s^{-1}) (Shi et al., 2012c).

Ferrozine analysis revealed that comparable concentrations of $Fe(II)_{aq}$ were produced for GT and HT (Figures 1C and 3D), confirming that HT reduction by $FMNH_2$ was minimal over the experimental period. Thus, an equivalent concentration of $MV^{+\bullet}$ (≤ 22 μM) was available for reaction with GT and HT yielding an equivalent $Fe(II)_{aq}$ concentration. For LEP, the measured [$Fe(II)_{aq}$] was the same as the starting concentration of $MV^{+\bullet}$; $MV^{+\bullet}$ reduced LEP quantitatively (Figure 4D). LEP reduction in the presence of FMN apparently involved both direct reaction with electron conduit MtrABC, and secondary reaction with $FMNH_2$.

3.3.2 Type II Experiments The reduction of HT and LEP in the presence of 10 μM $FMNH_2$ and the remaining encapsulated $MV^{+\bullet}$ (≤ 22 μM giving the starting concentration)

followed the same trend observed for GT, except with higher initial rates and, in case of LEP, a much larger extent of reduction (Figures 3A, 4A and Table 2). The oxidation of ~ 90% of the $MV^{+\bullet}$ occurred within a few seconds in the MELs-$FMNH_2$-LEP suspension (Figure 4A). In comparison, over 100 seconds was necessary to reach the same reaction extent under similar conditions using MELs or $FMNH_2$ alone (Figure 4A and Figure 1 in ref. (Shi et al., 2012c)). Such rate enhancement was consistent with the observations made for the MELs + GT + $FMNH_2$ system, and further confirmed that $FMNH_2$ enhanced MtrCAB electron transfer to Fe(III)-oxides.

In contrast to its rate enhancing effect on the initial reaction, the presence of $FMNH_2$ reduced the second stage reaction rates by factors of four and fifteen for HT and LEP, respectively, as compared to rates in the absence of FMN (Table S1). Similar trends were observed in the second-order bimolecular rate constants (Table S2).

The concentration profiles of FMN (Fig. 3C) and the evolved Fe(II) concentration (Fig. 3D) showed little evidence for $FMNH_2$ reaction with HT. In contrast, LEP reduction in the Type II experiment was coupled to $FMNH_2$ oxidation (Figure 4C) which occurred rapidly between 5 and 100 seconds after $MV^{+\bullet}$ was exhausted by LEP reduction. All of the $FMNH_2$ (10 μM) was oxidized by the completion of the experiment (440 seconds), albeit at decreasing rate (Fig. 4C). In the end, [Fe(II)] was close to the initial $MV^{+\bullet}$ concentration ($\leq$ 42 μM) (Figure 4D), indicating that all electron equivalents originally present in $MV^{+\bullet}$ were transferred to LEP through a combination of direct reaction with MtrCAB and parallel reaction with $FMNH_2$. This was not the case for either the GT or HT systems.

4. DISCUSSION

4.1 Thermodynamic and kinetic relationships

Nernst equation calculations indicated that $MV^{\bullet+}$ oxidation by FMN and all three Fe(III)-oxides should be quantitative under the experimental conditions used. Similar calculations predicted that the oxidation of $FMNH_2$ by the Fe(III)-oxides should also be close to 100% (Table S3). Consistent with these calculations, the oxidation of $MV^{\bullet+}$ in the MELs system was complete within ~ 400 seconds for all systems studied (Figures 1-4). However, the stoichiometric reduction of Fe(III)-oxides by $FMNH_2$, once formed, was only observed for LEP (Table 2) because of kinetic constraints. The concentration of Fe(II) for both GT and HT was below thermodynamic expectation given measured concentrations of $FMNH_2$. Calculations with previously reported initial rates of Fe(III) oxide reductive dissolution by $FMNH_2$ (Shi et al., 2013) suggested that only 3.2 μM and 0.4 μM Fe(II) should be produced in 400 seconds for the reaction with HT and GT, respectively, while the reaction with LEP would be complete. The production of $Fe(II)_{(aq)}$ from the reaction of $FMNH_2$ with GT or HT was less than the calculated values in our experiments because only a portion of the reactions proceeded at the initial rate, and there was less $FMNH_2$ in the present system (typically ≤ 10 μM) than used for the initial rate measurement (Shi et al., 2013). Consequently, $FMNH_2$, which was rapidly produced from FMN by the MELs, functioned as an electron sink in the GT and HT systems because of its relatively slow kinetic reactivity with these two more stable Fe(III) oxides. As will be discussed below, the thermodynamic driving force is more favorable for reaction between $FMNH_2$ and LEP.

Generally, a larger redox reaction free energy (i.e., greater difference between the effective reduction potentials of oxidant and reductant) for similar reactants leads to a faster reaction rate (e.g. Shi et al., 2013). We have previously shown that the initial surface area normalized reduction rate of Fe(III)-oxide by $FMNH_2$ increased with increases in the reduction

potential of the Fe(III)-oxide phase (0.001 $\mu mol \cdot m^{-2} \cdot s^{-1}$ for GT, 0.008 $\mu mol \cdot m^{-2} \cdot s^{-1}$ for HT, and 1.1 $\mu mol \cdot m^{-2} \cdot s^{-1}$ for LEP) (Shi et al., 2012c; Shi et al., 2013). For Fe(III)-oxide reduction by aqueous $MV^{\bullet+}$, the surface area normalized reduction rate increased from 1.36 $\mu mol \cdot m^{-2} \cdot s^{-1}$ for GT, to 2.63 $\mu mol \cdot m^{-2} \cdot s^{-1}$ for HT, and to 6.1 $\mu mol \cdot m^{-2} \cdot s^{-1}$ for LEP (White et al., 2013). These data also showed that the higher reduction potential of $FMNH_2$ (-0.216 V) compared to that of $MV^{\bullet+}$ (-0.450 V) led to significantly lower initial reduction rates of a given Fe(III)-oxide by $FMNH_2$ as compared by $MV^{\bullet+}$ at the same Fe(III)-oxide concentration. The initial surface area normalized rates for the Type II experiments presented herein where Fe(III)-oxides reacted with ≤ 22 µM of encapsulated $MV^{\bullet+}$ and 10 µM $FMNH_2$, followed the same order as expected from the reduction potentials (4.73 $\mu mol \cdot m^{-2} \cdot s^{-1}$ for GT < 11.10 $\mu mol \cdot m^{-2} \cdot s^{-1}$ for HT < 11.21 $\mu mol \cdot m^{-2} \cdot s^{-1}$ for LEP; Table 2). Therefore, thermodynamic driving force is a key factor in our experimental system, with the differences between $MV^{\bullet+}$ and $FMNH_2$ being especially important in determining the kinetic competence of $FMNH_2$ to act as a parallel reductant to $MV^{\bullet+}$/MtrCAB. However, the thermodynamic driving force of $MV^{\bullet+}$ is propagated through the MtrCAB complex which is limited in concentration (≤ 1 nM) and gated by intra- and inter-proteins heme arrangement to function over a specified redox window (e.g., ~ 0.400 V to 0.000 V). Due to the large concentration differences between the encapsulated $MV^{\bullet+}$ and the MtrCAB complex embedded on the liposome surface, the effective reduction potential (E') of the MELs are expected to be near the lowest reduction potential of the MtrCAB complex (i.e. -0.400 V;(Hartshorne et al., 2009)).

A single MR-1 cell has been estimated to contain approximately 1.2×10^{-19} moles of the MtrCAB complex (Ross et al., 2009). Thus, a typical *Shewanella* culture with 10^{10} cells/L may contain 1.2 nM MtrCAB, which is similar to the MtrCAB concentration in our MEL system.

Our model system consequently mimics select features of the Mtr pathway, with similar concentrations of the electron transfer complex MtrCAB as found in MR-1 cultures. However, the periplasmic reduction potential of *Shewanella* is driven by the redox couple NAD^+/NADH with a mid-point potential of -0.320 V (White et al., 2013) at sustainable µM-level concentrations (Wimpenny and Firth, 1972). The significantly lower reduction potential of $MV^{\bullet+}$ as compared to NADH along with an initial reductant concentration (e.g., ~42 µM) that was higher than the cytoplasmic electron pool provided a large thermodynamic driving force for reduction (of both FMN and Fe(III)-oxides) in our system relative to whole cells. The resulting Fe(III)-oxide reduction rates for the MELs were consequently higher than observed for whole cells or in-vitro studies with isolated *c*-Cyts or (Coursolle et al., 2010; Lies et al., 2005; von Canstein et al., 2008) because of thermodynamic, reactant concentration, and other effects.

4.2 Reaction pathways

Our results suggest that $FMNH_2$ may play multiple roles in the reduction of Fe(III)-oxides by the Mtr pathway. The overall kinetic behavior of the MELs + FMN + Fe(III) oxide system is interpreted to result from four fundamental kinetic reactions that occur at different rates (Figure 5). FMN reacts rapidly with $MV^{\bullet+}$ through the MtrCAB complex to form $FMNH_2$ and activated complex MtrABC-(FMN) in Reaction 1. This step transfers a portion of the electron equivalents from $MV^{\bullet+}$ to FMN. In Reaction 2, a portion of the remaining electron equivalents from $MV^{\bullet+}$ are transferred to Fe(III) oxide through the activated MtrCAB-(FMN) complex at an enhanced rate relative to the reaction between MELs and Fe-oxide (Reaction 3), which proceeds in parallel. Stored electron equivalents in $FMNH_2$ are the last to react with the Fe(III) oxides in Reaction 4, where significant reaction progress was noted only for LEP because of thermodynamic constraints. Reaction of $FMNH_2$ with GT and HT would have been observed

after significantly longer time periods. Differences between the kinetic behaviors of the three oxides in the ternary system can be rationalized by the noted range in the four reaction rates (Fig. 5). Several aspects of these reaction sequences warrant additional discussion.

A significant observation was that $FMNH_2$ at low concentration (≤ 1 μM) accelerates the initial electron transfer rate to all three Fe(III) oxides studied by a factor of five or more over that in the absence of $FMNH_2$ (Table 2). The initial reduction rates for all three phases followed the order of MELs + $FMNH_{2(aq)}$ > $MV^{\bullet+}_{(aq)}$ > MELs >> $FMNH_2$ (Figure 6). Our interpretation of this results is that a molecular interaction between FMN (or its reduced species $FMNH^{\bullet}$, or $FMNH_2$) and MtrCAB [e.g. (FMN) in Fig. 5] leads to rate enhancement. Crystal structure determinations for MtrF, a homologue of MtrC, suggested the presence of two flavin binding domains (per MtrF molecule) near the heme core that could be involved in such interaction (Clarke et al., 2011). A specific, but as yet unidentified species of FMN may consequently serve as a co-factor for MtrC as suggested by Okamoto et al (Okamoto et al., 2013) during the initial stage of Fe(III)-oxide reductive dissolution. It is currently unclear what factors control the overall extent of electron transfer through the activated complex [*e.g.* moles of Fe(II) produced through Reaction 2].

Saturation of the flavin binding domain is anticipated at low $FMNH_2$ concentrations given the nano-molar concentration of MtrCAB in the MELs and the existence of only two FMN binding domains on each MtrCAB complex (Clarke et al., 2011). Domain saturation is consistent with the observed trend that no further enhancement in initial rate was observed at $[FMNH_2] \geq 1$ μM. Measured extracellular flavin concentrations in anaerobic cell culture medium of *Shewanella* are typically in the sub-micromolar range (Ross et al., 2009; von Canstein et al., 2008), indicating that only low flavin concentrations are necessary for

enhancement of reductive dissolution rates by whole cells. Enhanced reaction rates have been observed for other co-factors, such as Mn(II) and Ni(II) for bacterial protein phosphatases (Shi et al., 2001).

FMN concentrations in excess of one micromolar inhibited Fe(III)-oxide reduction during the second, slower reaction stage. FMN exerted brief, yet significant initial rate enhancement at 2 nM and 10 nM (Figure 2A, B). After that, the reaction kinetics were almost identical to those in the absence of FMN, except for a concentration decrease in $MV^{\bullet+}$ that corresponded to the amount reacted during the initial stage. Beginning at [FMN] = 1 μM, where the initial reaction rate peaked, the second stage became slower as compared to that in the absence of $FMNH_2$, and inhibition become more pronounced as the $FMNH_2$ concentration was increased. The inhibition effect was common to all three Fe(III)-oxides based on data at 10 μM $FMNH_2$ (Figures 2-4 and Table S1).

One possible explanation for the observed inhibition effect was $FMNH_2$ adsorption on Fe(III)-oxide. Flavins strongly adsorb to Fe/Mn-oxides, carbon electrodes, gold nanoparticles, and bacteria cell surfaces (Marsili et al., 2008; Shi et al., 2012c). Assuming a molecular diameter of 1.3 nm for $FMNH_2$, we estimated that a monolayer of $FMNH_2$ on goethite might contain 2.1×10^{17} $FMNH_2$ molecules (the equivalent of 3.3×10^{-7} M $FMNH_2$), which is within the range of concentrations studied here. The formation of a surface complex between phosphate groups on FMN or $FMNH_2$ and surface Fe(III) is plausible (Mortland et al., 1984) and might restrict access of exposed MtrC to the Fe(III)-oxide through steric and/or electrostatic interaction.

5. CONCLUSIONS AND IMPLICATIONS

The present study revealed that microbially produced FMN may play multiple roles in the microbial reduction of Fe(III)-oxides. These roles include function as: 1) a co-factor to MtrC enhancing its electron transfer (to all Fe(III) oxides), 2) a parallel reductant serving as an electron shuttle to the Mtr pathway (lepidocrocite only), and 3) an "unreactive" electron sink over the experimental time period (goethite and hematite). The latter two roles were determined and constrained by the aqueous reductive dissolution rates of $FMNH_2$with the individual Fe(III) oxides. Through possible specific interaction between MtrCAB and FMN/$FMNH_2$, $FMNH_2$ enhanced electron transfer rates between the MELs and Fe(III)-oxides by a factor of 3.4, 4.2 and 1.8 for GT, HT and LEP, respectively, compared to that by aqueous $MV^{\bullet+}$. Such enhancement was optimized at sub-micromolar FMN concentrations, a level commonly observed in whole cell cultures under anaerobic conditions.

Many natural systems contain ferrihydrite as the predominant Fe(III) oxide. It is a nano-crystalline phase (Jambor and Dutrizac, 1998) that is a stronger oxidant than lepidocrocite. Ferrihydrite is rapidly dissolved by FMN (Shi et al., 2012c). It was not studied here because of its strong tendency to recrystallize to more stable Fe(III) oxide phases (goethite and lepidocrocite) in presence of Fe(II) (Yee et al., 2006; Zachara et al., 2011). We suspect that ferrihydrite reduction would be greatly enhanced over that observed for lepidocrocite by the parallel reactions of MELs and reduced flavin (e.g. $FMNH_2$).

The behavior of the MtrCAB/FMN/Fe(III) oxide system was strongly dependent on 1) the physiologic redox potential that poises the MtrCAB complex, and 2) the half-cell potential of the Fe(III) oxide phase that regulates the relative reaction rates with redox-poised *c*-Cyt and FMN. The concentration ratios of reductants (MEL- $MV^{\bullet+}$) to oxidants [Fe(III) oxide], and the concentration of the electron transfer conduit (MtrABC) were also important. These same

dependencies are expected for whole cell and natural systems, with additional complexities increasing with observational scale. For FMN-enhanced Fe(III)-oxide reduction by MELs, the surface normalized initial rates at 10 µM FMN varied within a factor of three between goethite (4.73 µmol m^{-2} s^{-1}), hematite (11.10 µmol m^{-2} s^{-1}), and lepidocrocite (11.21 µmol m^{-2} s^{-1}). Yet, for Fe(III)-oxide reduction by $FMNH_2$, the same rates varied over three orders of magnitude from ~0.001 µmol m^{-2} s^{-1} for goethite to 1.1 µmol m^{-2} s^{-1} for lepidocrocite. Additional research is required to determine whether these striking differences are thermodynamically or mechanistically controlled, and how these findings relate to natural systems.

Liposomes encapsulating reductants with redox potentials near that of NADH are now being tested to constrain model system studies to a physiologically relevant redox window. Outer membrane vesicles (Schooling and Beverage, 2006; Kim et al., 2007; Pirbadian et al., 2014) are also being considered with redox properties closer to in vivo conditions. Through the use of physiologically relevant reductants and membrane systems, additional insights on the kinetic mechanisms of Fe(III)-oxide reduction by DIRB can be gained.

SUPPORTING INFORMATION. Four figures and three tables.

ACKNOWLEDGMENTS

This research was supported by the Geoscience Research Program of the Office of Basic Energy Science (BES), U.S. Department of Energy (DOE). The contribution of Jim Fredrickson and Liang Shi were supported by Pacific Northwest National Laboratory Scientific Focus Area (PNNL SFA). Part of this research was performed at EMSL, a national scientific user facility at PNNL managed by the Department of Energy's Office of Biological and Environmental

Research. Pacific Northwest National Laboratory is operated for the U.S. Department of Energy by Battelle under Contract DE-AC06-76RLO 1830.

Table 1. Relevant properties of Fe-oxides in this work[a].

Iron oxides	One-electron reduction half reaction (relevant ΔG_f^o and ΔG^o values are provided under each species)	Redox potentials [b] (mV)		BET surface area ($m^2 \cdot g^{-1}$)	pH_{zpc} [c]
		E^o	E'		
Goethite	$\alpha FeOOH(s) + 3H^+ + e^- = Fe^{2+} + 2H_2O$	727	-158	38	7.5-9.5
Hematite	$\alpha Fe_2O_3(s) + 6H^+ + 2e^- = 2Fe^{2+} + 3H_2O$	764	-121	34	7.5-9.5
Lepidocrocite	γ-$FeOOH(s) + 3H^+ + e^- = Fe^{2+} + 2H_2O$	781	-104	130	6.7-7.5

[a] See Zhi et al (Shi et al., 2012c; Shi et al., 2013) for the basis of the thermodynamic values and morphological characterization results. [b] Calculated using $E^o = -\Delta G^o/nF$, and Nernst equation. Faraday constant F = 96.485 kJ per volt gram equivalent. E': pH 7.0, 1 μM total dissolved iron. [c] From (Cornell and Schwertmann, 2003), page 235.

Table 2. Initial reaction rates of Fe-oxide reduction by $MV^{+\bullet}$-encapsulated proteoliposomes in Type I and Type II reaction schemes at various initial flavin mononucleotide (FMN) concentrations at 25 C. 200 μM Fe(III) oxide, 40 μM $MV^{+\bullet}$, 50 mM HEPES buffer (pH 7.0) containing 2 mM $CaCl_2$ and 10 mM KCl. Fe(III) oxides include goethite (GT), hematite (HT) and lepidocrocite (LEP).

Mineral	[FMN] (μM)	Initial rate ($\mu M \cdot s^{-1}$)	Surface area normalized initial rate ($\mu mol \cdot m^{-2} \cdot s^{-1}$)	Steady state $[Fe^{II}_{aq}]$ (μM) [a,b]
Type I Experiment				
None	10.0	54.33±3.73	-	-
GT	0.0	0.59±0.07	0.88±0.10	35.3±1.0(40.0)
	1.0	10.28±2.82[c]	15.23±4.18	32.8±1.7(38.0)
	10.0	56.83±25.67[c]	84.19±38.03	13.4±0.4(20.0)
	20.0	53.51±23.64[c]	79.27±35.02	2.0±0.1(0.0)
HT	0.0	0.97±0.11	1.78±0.21	37.1±0.3(40.0)
	10.0	42.90±3.29[c]	63.56±4.87	15.4±1.1(20.0)
LEP	0	5.43±1.39	2.35±0.60	37.0±3.7(40.0)
	10.0	77.51±5.58[c]	33.56±2.42	41.0±1.2(20.0)
Type II Experiment				
GT	0.002	3.29±0.70	4.87±1.04	33.3±1.1(40.0)
	0.01	3.39±1.15	5.02±1.71	33.1±3.0(40.0)
	1.0	8.74±0.79	12.95±1.17	30.0±2.8(38.0)
	10.0	3.20±0.54	4.73±0.79	15.2±3.3(20.0)
	20.0	-	-	2.6±0.6(0.0)
HT	10.0	6.03±0.32	11.10±0.58	14.0±0.2(20.0)
LEP	10.0	25.90±5.93	11.21±2.57	38.8±0.9(20.0)

[a] value in parenthesis is the expected value based on reactant stoichiometries.

[b] Calculated using E^o (hematite) = 764 mV (Shi et al., 2013).

[c] Initial rates in these Type I experiments are dominated by FMN reduction by MELs.

REFERENCES

Breuer, M., Rosso, K. M., and Blumberger, J. (2014) Electron flow in multiheme bacterial cytochromes is a balancing act between heme electronic interaction and redox potentials. *Proc. Natl. Acad. Sci. USA* **111**, 611-616.

Brutinel, E. D. and Gralnick, J. A. (2012) Shuttling happens: soluble flavin mediators of extracellular electron transfer in Shewanella. *Appl. Microbiol. Biot.* **93**, 41-48.

Clarke, T. A., Edwards, M. J., Gates, A. J., Hall, A., White, G. F., Bradley, J., Reardon, C. L., Shi, L., Beliaev, A. S., Marshall, M. J., Wang, Z., Watmough, N. J., Fredrickson, J. K., Zachara, J. M., Butt, J. N., and Richardson, D. J. (2011) Structure of a bacterial cell surface decaheme electron conduit. *Proc. Natl. Acad. Sci. USA* **108**, 9384-9389.

Cornell, R. M. and Schwertmann, U. (2003) *The Iron Oxides: Structure, Properties, Reactions, Occurrences, and Uses.* Wiley, Weinheim.

Coursolle, D., Baron, D. B., Bond, D. R., and Gralnick, J. A. (2010a) The Mtr respiratory pathway is essential for reducing flavins and electrodes in *Shewanella oneidensis*. *J Bacteriol* **192**, 467-474.

Hartshorne, R. S., Reardon, C. L., Ross, D., Nuester, J., Clarke, T. A., Gates, A. J., Mills, P. C., Fredrickson, J. K., Zachara, J. M., Shi, L., Beliaev, A. S., Marshall, M. J., Tien, M., Brantley, S., Butt, J. N., and Richardson, D. J. (2009a). Characterization of an electron conduit between bacteria and the extracellular environment. *Proc. Natl. Acad. Sci. USA* **106**, 22169-22174.

Jambor, J. L. and Dutrizac, J. E. (1998) Occurrence and constitution of natural and synthetic ferrihydrite, a widespread iron oxyhydroxide. *Chemical Reviews* **98**, 2549-2585.

Kim, J.-Y., Doody, A.M., Chen, D.J., Cremona, G.H., Shuler, M.L., Putnam, D., and DeLisa, M.P. (2008) Engineered Bacterial Outer Membrane Vesicles with Enhanced Functionality. *J. Mol. Biol.* **380**, 51-66.

Lies, D. P., Hernandez, M. E., Kappler, A., Mielke, R. E., Gralnick, J. A., and Newman, D. K. (2005) Shewanella oneidensis MR-1 uses overlapping pathways for iron reduction at a distance and by direct contact under conditions relevant for biofilms. *Appl. Environ. Microbiol.* **71**, 4414-4426.

Liu, Y., Wang, Z., Liu, J., Levar, C., Edwards, M., Babauta, J. T., Kennedy, D. W., Shi, Z., Beyenal, H., Bond, D. R., Clarke, T. A., Butt, J. N., Richardson, D. J., Rosso, K. M., Zachara, J. M., Fredrickson, J. K., and Shi, L. (2014) A trans-outer membrane porin-cytochrome protein complex for extracellular electron transfer by Geobacter sulfurreducens PCA. *Environ. Microbiol. Rep.* (doi: 10.1111/1758-2229.12204).

Lovley, D. R. (1991) Dissimilatory Fe(III) and Mn(IV) reduction. *Microbiol. Rev.* **55**, 259-287.

Lovley, D. R., Stolz, J. F., Nord, G. L., and Phillips, E. J. P. (1987) Anaerobic production of magnetite by a dissimilatory iron-reducing microorganism. *Nature* **330**, 252-254.

Marsili, E., Baron, D. B., Shikhare, I. D., Coursolle, D., Gralnick, J. A., and Bond, D. R. (2008) Shewanella Secretes flavins that mediate extracellular electron transfer. *Proc. Natl. Acad. Sci. USA* **105**, 3968-3973.

Mortland, M. M., Lawless, J. G., Hartman, H., and Frankel, R. (1984) Smectite interactions with flavomononucleotid. *Clays Clay Miner.* **32**, 279-282.

Myers, C. R. and Nealson, K. H. (1988) Bacterial manganese reduction and growth with manganese oxide as the sole electron-acceptor. *Science* **240**, 1319-1321.

Myers, C. R. and Nealson, K. H. (1990) Respiration-linked proton translocation coupled to anaerobic reduction of manganese(IV) and iron(III) in shewanella-putrefaciens MR-1. *J. Bacteriol.* **172**, 6232-6238.

Okamoto, A., Hashimoto, K., Nealson, K. H., and Nakamura, R. (2013) Rate enhancement of bacterial extracellular electron transport involves bound flavin semiquinones. *Proc. Natl. Acad. Sci. USA* **110**, 7856-7861.

Pirbadian, S., Barchinger, S.E., Leung, K.M., Byun, H.S., Jangir, Y., Bouhenni, R.A., Reed, S.B., Romine, M.F., Saffarini, D.A., Shi, L., Gorby, Y.A., Golbeck, J.H., and El-Naggar, M.Y. (2014) Shewanella Oneidensis Mr-1 Nanowires Are Outer Membrane and Periplasmic Extensions of the Extracellular Electron Transport Components. *Proc. Natl. Acad. Sci. USA* **111**, 12883-12888.

Richardson, D. J., Butt, J. N., Fredrickson, J. K., Zachara, J. M., Shi, L., Edwards, M. J., White, G., Baiden, N., Gates, A. J., Marritt, S. J., and Clarke, T. A. (2012) The porin-cytochrome' model for microbe-to-mineral electron transfer. *Mol. Microbiol.* **85**, 201-212.

Roden, E. E. and Zachara, J. M. (1996) Microbial reduction of crystalline iron(III) oxides: Influence of oxide surface area and potential for cell growth. *Environ. Sci. Technol.* **30**, 1618-1628.

Ross, D. E., Brantley, S. L., and Tien, M. (2009) Kinetic Characterization of OmcA and MtrC, Terminal Reductases Involved in Respiratory Electron Transfer for Dissimilatory Iron Reduction in Shewanella oneidensis MR-1. *Appl. Environ. Microbiol.* **75**, 5218-5226.

Ross, D. E., Ruebush, S. S., Brantley, S. L., Hartshorne, R. S., Clarke, T. A., Richardson, D. J., and Tien, M. (2007) Characterization of protein-protein interactions involved in iron reduction by Shewanella oneidensis MR-1. *Appl. Environ. Microbiol.* **73**, 5797-5808.

Schwertmann, U. and Cornell, R. M. (2000) *Iron oxides in the laboratory preparation and characterization*. Wiley-VCH, Wiley-VCH.

Schooling, S.R. and Beveridge, T.J. (2006) Membrane Vesicles: An Overlooked Component of the Matrices of Biofilms. J. Bacteriol. **188**, 5945-5957.

Shi, L., Kehres, D. G., and Maguire, M. E. (2001) The PPP-family protein phosphatases PrpA and PrpB of Salmonella entetica serovar typhimurium possess distinct biochemical properties. *J. Bacteriol.* **183**, 7053-7057.

Shi, L., Rosso, K. M., Clarke, T. A., Richardson, D. J., Zachara, J. M., and Fredrickson, J. K. (2012a) Molecular underpinnings of Fe(III) oxide reduction by Shewanella oneidensis MR-1. *Frontiers in Microbiology* **3**. Article 50:1-10.

Shi, L., Rosso, K. M., Zachara, J. M., and Fredrickson, J. K. (2012b) Mtr extracellular electron-transfer pathways in Fe(III)-reducing or Fe(II)-oxidizing bacteria: a genomic perspective. *Biochem Soc Trans* **40**, 1261-7.

Shi, L., Squier, T. C., Zachara, J. M., and Fredrickson, J. K. (2007) Respiration of metal (hydr)oxides by *Shewanella* and *Geobacter*: a key role for multihaem *c*-type cytochromes. *Mol. Microbiol.* **65**, 12-20.

Shi, Z., Zachara, J. M., Shi, L., Wang, Z., Moore, D. A., Kennedy, D. W., and Fredrickson, J. K. (2012c) Redox Reactions of Reduced Flavin Mononucleotide (FMN), Riboflavin (RBF), and Anthraquinone-2,6-disulfonate (AQDS) with Ferrihydrite and Lepidocrocite. *Environ. Sci. Technol.* **46**, 11644-11652.

Shi, Z., Zachara, J. M., Wang, Z., Shi, L., and Fredrickson, J. K. (2013) Reductive dissolution of goethite and hematite by reduced flavins. *Geochim. Cosmochim. Acta* **121**, 139-154.

Stookey, L. L. (1970) Ferrozine - A new spectrophotometric reagent for iron. *Anal. Chem.* **42**, 779-781.

Stumm, W., Furrer, G., Wieland, E., and Zinder, B. (1985) The effects of complex-forming ligands on the dissolution of oxides and aluminosilicates. In: Drever, J. I. (Ed.),*The Chemistry of Weathering*. D. Reidel, Dordrecht, The Netherlands.

Torrent, J., Schwertmann, U., and Barron, V. (1987) The reductive dissolution of synthetic goethite and hematite in dithionite. *Clay Miner.* **22**, 329-337.

von Canstein, H., Ogawa, J., Shimizu, S., and Lloyd, J. R. (2008) Secretion of flavins by Shewanella species and their role in extracellular electron transfer. *Appl. Environ. Microbiol.* **74**, 615-623.

Wang, Y. and Newman, D. K. (2008) Redox reactions of phenazine antibiotics with ferric (hydr)oxides and molecular oxygen. *Environ. Sci. Technol.* **42**, 2380-2386.

Wang, Z. M., Liu, C. X., Wang, X. L., Marshall, M. J., Zachara, J. M., Rosso, K. M., Dupuis, M., Fredrickson, J. K., Heald, S., and Shi, L. (2008b) Kinetics of Reduction of Fe(III) Complexes by Outer Membrane Cytochromes MtrC and OmcA of Shewanella oneidensis MR-1. *Appl. Environ. Microbiol.* **74**, 6746-6755.

White, G. F., Shi, Z., Shi, L., Dohnalkova, A. C., Fredrickson, J. K., Zachara, J. M., Butt, J. N., Richardson, D. J., and Clarke, T. A. (2012) Development of a proteoliposome model to probe transmembrane electron-transfer reactions. *Biochem. Soc. Trans.* **40**, 1257-1260.

White, G. F., Shi, Z., Shi, L., Wang, Z., Dohnalkova, A. C., Marshall, M. J., Fredrickson, J. K., Zachara, J. M., Butt, J. N., Richardson, D. J., and Clarke, T. A. (2013) Rapid electron exchange between surface-exposed bacterial cytochromes and Fe(III) minerals. *Proc. Natl. Acad. Sci. USA* **110**, 6346-51.

Wimpenny, J. W. and Firth, A. (1972) Levels of nicotinamide adenine dinucleotide and reduced nicotinamide adenine dinucleotide in facultative bacteria and the effect of oxygen. *J. Bacteriol.* **111**, 24-32.

Wu, C., Cheng, Y.-Y., Li, B.-B., Li, W.-W., Li, D.-B., and Yu, H.-Q. (2013) Electron acceptor dependence of electron shuttle secretion and extracellular electron transfer by Shewanella oneidensis MR-1. *Bioresource Technol.* **136**, 711-714.

Yee, N., Shaw, S., Benning, L. G., and Nguyen, T. H. (2006) The rate of ferrihydrite transformation to goethite via the Fe(II) pathway. *American Mineralogist* **91**, 92-96.

Zachara, J. M., Fredrickson, J. K., Smith, S. C., and Gassman, P. L. (2001) Solubilization of Fe(III) oxide-bound trace metals by a dissimilatory Fe(III) reducing bacterium. *Geochim. Cosmochim. Acta* **65**, 75-93.

Zachara, J. M., Kukkadapu, R. K., Peretyazhko, T., Bowden, M., Wang, C., Kennedy, D. W., Moore, D., and Arey, B. (2011) The mineralogic transformation of ferrihydrite induced by heterogeneous reaction with bioreduced anthraquinone disulfonate (AQDS) and the role of phosphate. *Geochim. Cosmochim. Acta* **75**, 6330-6349.

Figure captions

Figure 1. Kinetic data of GT reduction by MELs in the absence or presence of FMN at different concentrations in the Type I experiment. Reaction conditions: 40 μM $MV^{+\cdot}$, 200 μM GT, 50 mM HEPES buffer (pH 7.0). FMN concentrations: 0, 1, 10, and 20 μM. (A) $MV^{+\cdot}$ concentration as a function of time; (B) FMN concentration as a function of time with 10 μM initial FMN; (C) aqueous Fe^{2+} concentration measured at the end of kinetic experiment.

Figure 2. Kinetic data of GT reduction by MELs in the absence or presence of FMN at different concentrations, Type II experiment. Reaction conditions: 35 - 40 μM $MV^{+\cdot}$, 200 μM GT, 50 mM HEPES buffer (pH 7.0). FMN concentrations: 0, 0.002, 0.01, 1, 10, and 20 μM. (A) and (B) $MV^{+\cdot}$ concentration as a function of time after Fe(III) oxide addition, only show the step 2; (C) aqueous Fe^{2+} concentration measured at the end of kinetic experiment. The red arrow labeled $t_{2,0}$ points to the start time of the Type II reaction with GT.

Figure 3. Kinetic data of HT reduction by MELs in the absence or presence of 10 μM FMN in Type I and Type II experiments. Reaction conditions: 35 - 40 μM $MV^{+\cdot}$, 200 μM HT, 50 mM HEPES buffer (pH 7.0). (A) $MV^{+\cdot}$ concentration as a function of time. The red arrow labeled $t_{2,0}$ points to the start time of the type II reaction with HT. No FMN was added in control run; (B) FMN concentration as a function of time in Type I experiment; (C) FMN concentration as a function of time in Type II experiment at the second step; (D) aqueous Fe^{2+} concentration measured at the end of kinetic experiment.

Figure 4. Kinetic data of LEP reduction by MELs in the absence or presence of 10 μM FMN in Type I and Type II experiment. Reaction conditions: 35 - 40 μM $MV^{+\cdot}$, 200 μM LEP, 50 mM HEPES buffer (pH 7.0). (A) $MV^{+\cdot}$ concentration as a function of time. The red arrow labeled $t_{2,0}$ points to the start time of the Type II reaction with LEP. No FMN was added in control run. (B) FMN concentration as a function of time in Type I experiment; (C) FMN concentration as a function of time in Type II experiment at the second step; (D) aqueous Fe^{2+} concentration measured at the end of kinetic experiment.

Figure 5. Schematic representations of the reaction pathways for Fe(III)-oxide reduction by MELs in the presence of $FMNH_2$. (FMN) = cytochrome bound FMN. The overall kinetic behavior of the MELs + FMN + Fe(III) oxide system is the result of four fundamental kinetic reactions that occur at different rates: A) FMN reacts with MELs resulting $FMNH_2$ and MtrCAB-bound activated complex, MtrCAB-(FMN); B) Electron transfer via the MtrCAB-(FMN) leads to very fast reduction of Fe-oxide by MELs; C) In parallel, MELs reduce Fe(III)-oxide at intermediate to fast rates; and D) Fe-oxide reduction by $FMNH_2$ at slow to intermediate rate dictated by the thermodynamic driving forces.

Figure 6. Comparisons of the surface-normalized initial rates of Fe-oxide reductive dissolution by $MV^{\bullet+}$ encapsulated in proteoliposomes in the presence of 10 μM $FMNH_2$ (Type II experiment) in the present work with those by aqueous $MV^{\bullet+}$,[a] aqueous $FMNH_2$[b] and $MV^{\bullet+}$-encapsulated in proteoliposomes without $FMNH_2$[a] at pH 7.0. [a] Data from (White et al., 2013); [b] Data from (Shi et al., 2012c; Shi et al., 2013).

Figure

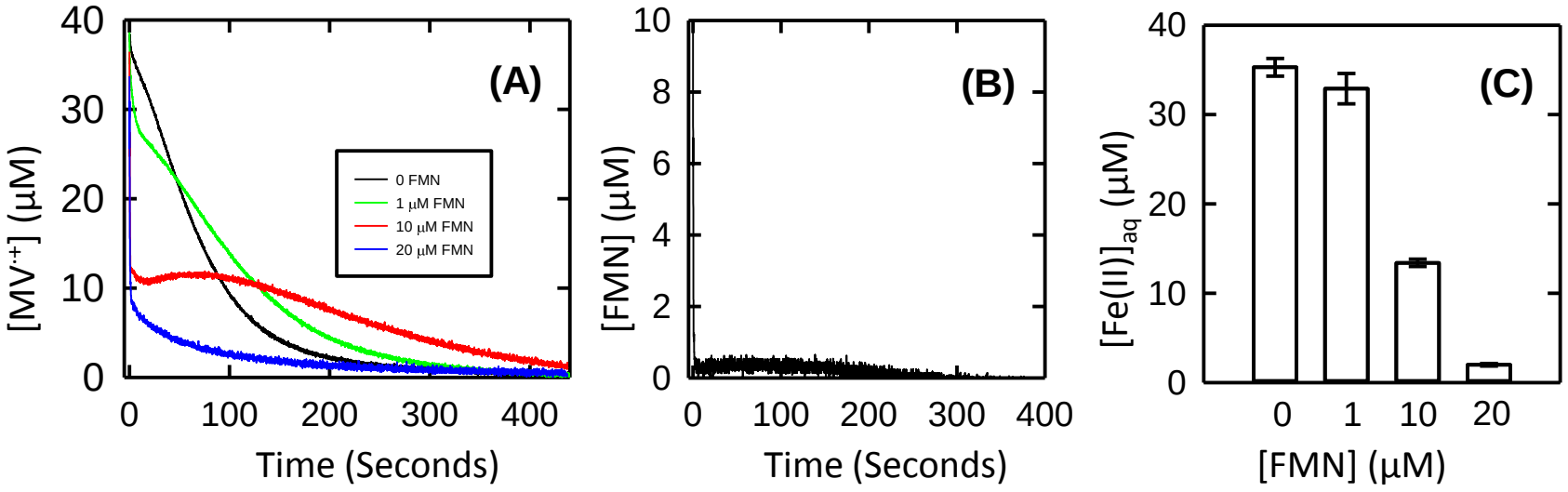

Wang et al Figure 1

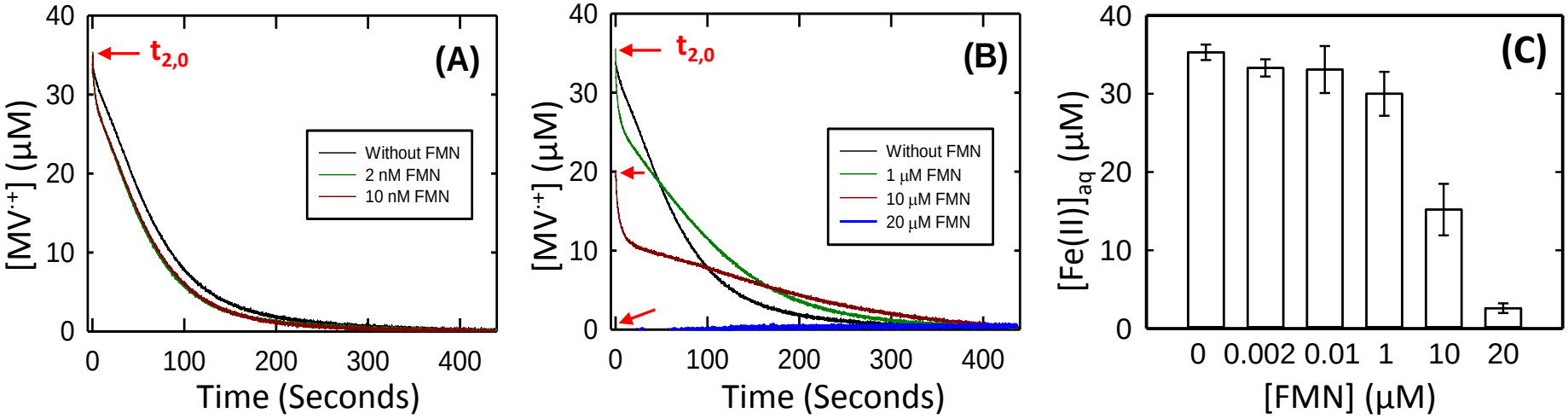

Wang et al Figure 2

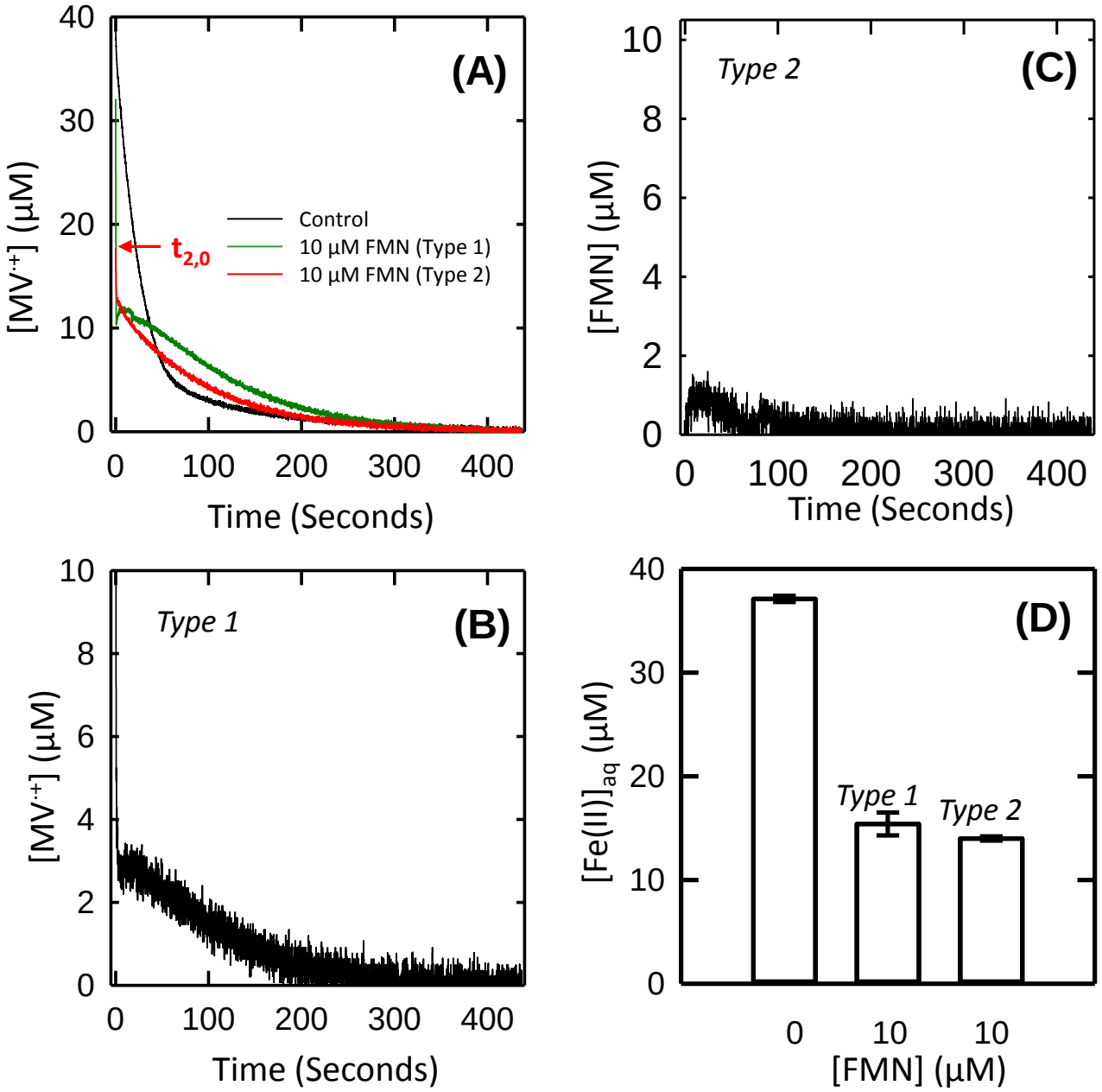

Wang et al Figure 3

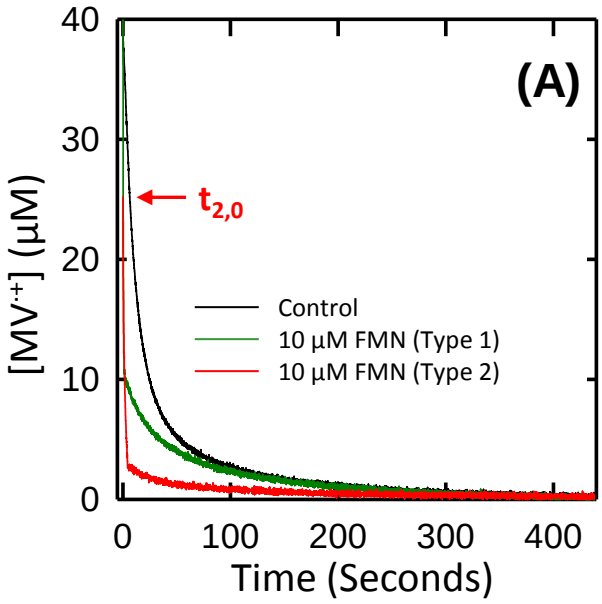

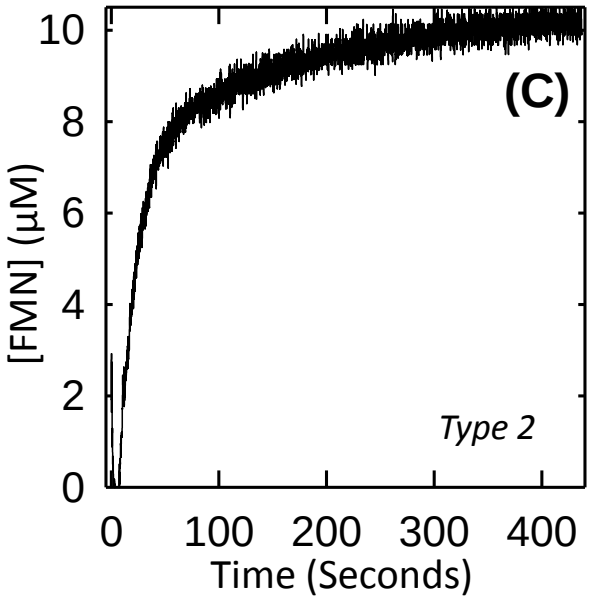

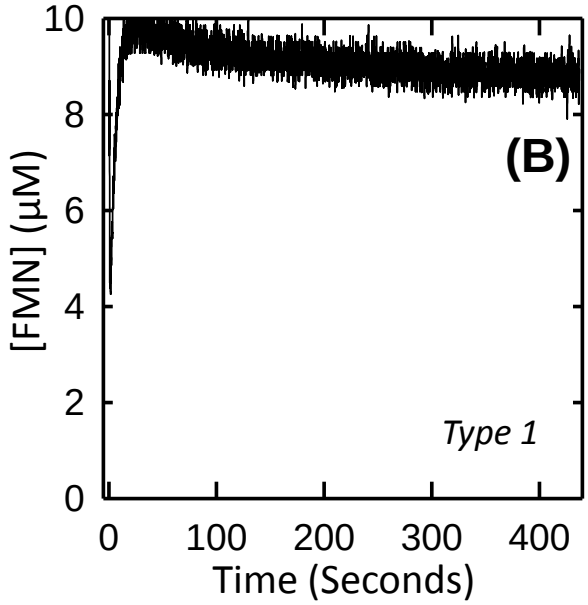

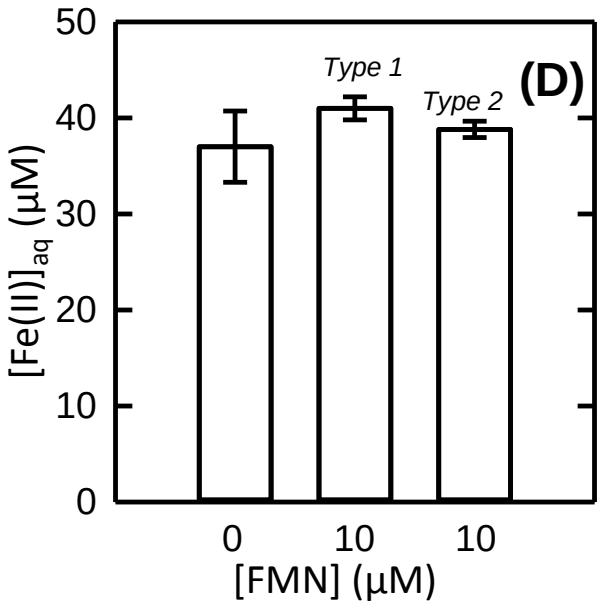

Wang et al Figure 4

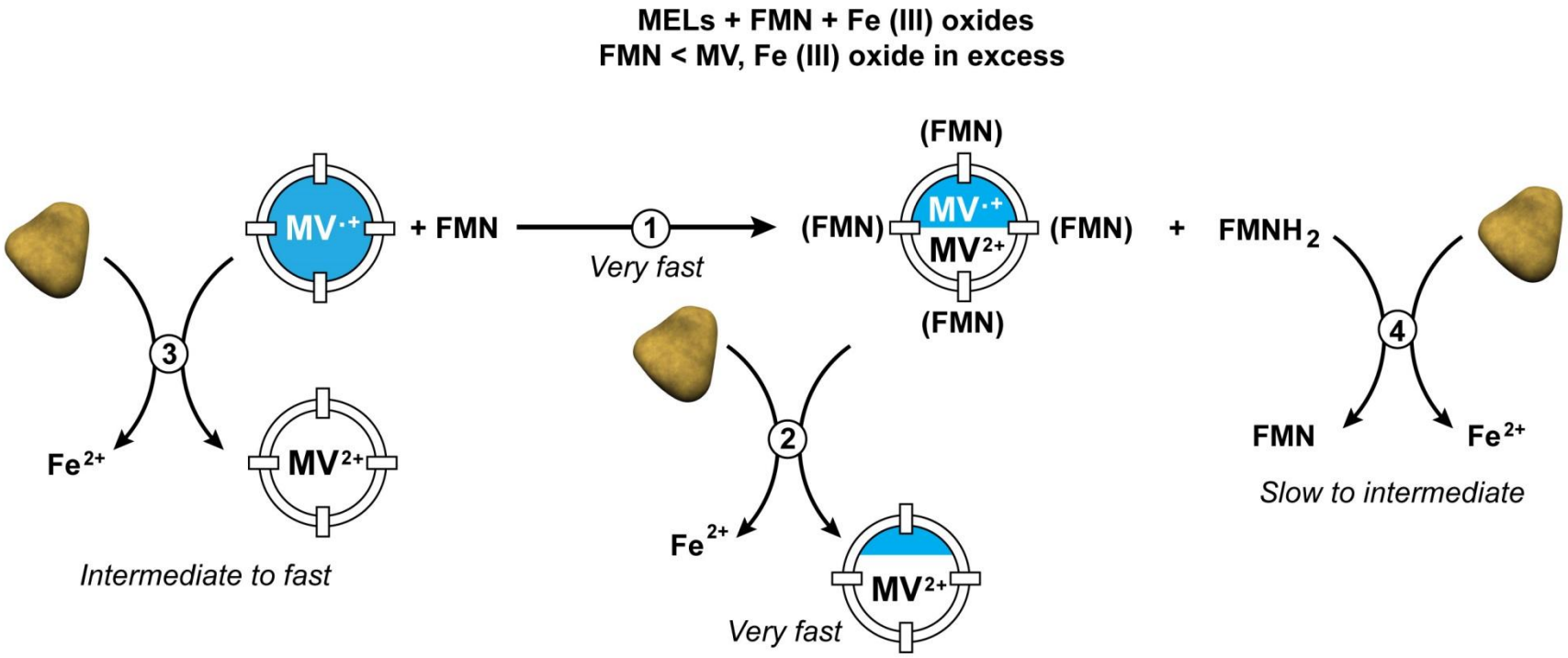

Wang et al Figure 5

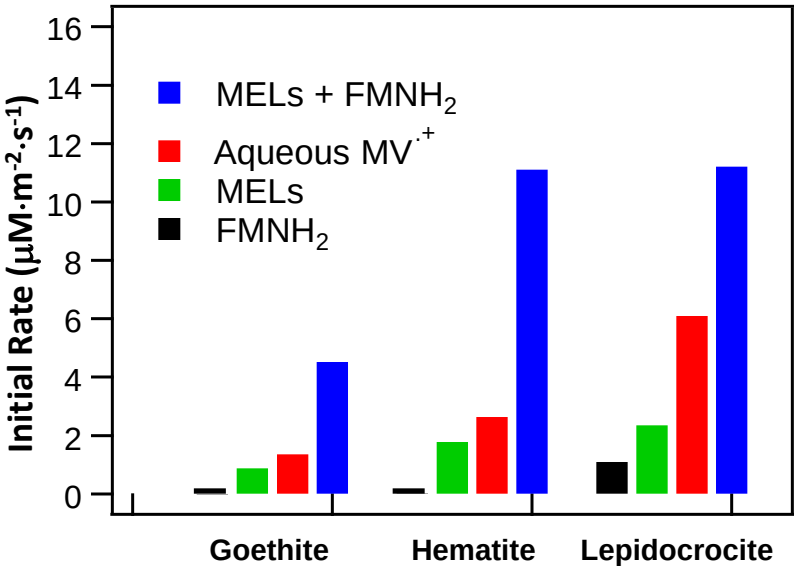

Wang et al Figure 6